Chemical Science

ROYAL SOCIETY OF CHEMISTRY

EDGE ARTICLE

View Article Online
View Journal | View Issue

Cite this: *Chem. Sci.*, 2023, **14**, 7753

All publication charges for this article have been paid for by the Royal Society of Chemistry

Received 17th March 2023
Accepted 31st May 2023

DOI: 10.1039/d3sc01411h

rsc.li/chemical-science

A path towards single molecule vibrational strong coupling in a Fabry–Pérot microcavity†

Arghadip Koner,[a] Matthew Du,[b] Sindhana Pannir-Sivajothi,[a] Randall H. Goldsmith[c] and Joel Yuen-Zhou*[a]

Interaction between light and molecular vibrations leads to hybrid light-matter states called vibrational polaritons. Even though many intriguing phenomena have been predicted for single-molecule vibrational strong coupling (VSC), several studies suggest that these effects tend to be diminished in the many-molecule regime due to the presence of dark states. Achieving single or few-molecule vibrational polaritons has been constrained by the need for fabricating extremely small mode volume infrared cavities. In this theoretical work, we propose an alternative strategy to achieve single-molecule VSC in a cavity-enhanced Raman spectroscopy (CERS) setup, based on the physics of cavity optomechanics. We then present a scheme harnessing few-molecule VSC to thermodynamically couple two reactions, such that a spontaneous electron transfer can now fuel a thermodynamically uphill reaction that was non-spontaneous outside the cavity.

Introduction

Strong coupling (SC) ensues when the rate of coherent energy exchange between the matter degrees of freedom (DOF) and a confined electromagnetic field exceeds the losses from either of them.[1–4] This interplay leads to the emergence of hybrid light-matter states called polaritons,[5–7] which inherit properties from both the photonic and the matter constituents. For molecular systems, due to the small magnitude of the transition dipole moment of most individual molecules, SC is typically achieved by having an ensemble of $N \gg 1$ molecules interact with a cavity mode.[5,8] In this collective case, in addition to two polariton states, SC leads to $(N-1)$ dark states which are predominantly molecular in character.[9] In both the electronic and vibrational regimes, harnessing these hybrid light-matter states has led to the emergence of a plethora of polariton-based devices[10] such as amplifiers,[11,12] tunneling diodes,[13] routers,[14] and ultrafast switches;[15,16] and novel phenomena like enhanced energy and charge transport,[17–19] modification and control of a chemical reaction without external pumping,[20,21] and remote catalysis.[22]

Theoretical models of polaritons often use a single molecule with a collective super radiant coupling to the cavity to explain the experimentally observed effects of collective SC on physical and chemical phenomena.[23–26] However, several theoretical studies, that account for the large number of molecules coupled to the cavity, suggest that SC could be rendered less effective in the collective regime owing to the entropic penalty from the dark states.[6,27,28] For enhanced polaritonic effects, the state-of-the-art is either to use polariton condensates[29,30] or to achieve single-molecule SC.[31] In the electronic regime, both polariton condensation[32–35] and single-molecule SC[31,36–38] have been achieved. There have been theoretical proposals of ways to achieve a vibrational polariton condensate.[39] However, to the best of our knowledge, in the vibrational regime, neither condensation nor single-molecule SC has yet been experimentally demonstrated. The bottleneck for single molecule SC in the vibrational case is the fabrication of low-mode volume cavities in the infrared (IR) regime.[40] This calls for alternate strategies to attain vibrational SC with a single or few molecules.

In this work, we propose using optomechanics as a way to achieve SC for molecular vibrations. Over the last decade, optomechanics has emerged as a powerful tool in quantum technologies with applications[41] such as backaction cooling of a mechanical oscillator,[42,43] parametric amplification,[44–46] optomechanically induced transparency,[47,48] and generation of non-classical quantum states.[49,50] Aspelmeyer and co-workers have demonstrated SC in an optomechanical architecture, for a micromechanical resonator coupled to an optical cavity setup.[51] It has been shown recently that surface-enhanced and cavity-enhanced Raman spectroscopy (SERS/CERS) can be understood through the theoretical framework of cavity optomechanics.[52–57] Here we exploit this observation to demonstrate that a single molecule in a CERS setup, under

[a]Department of Chemistry and Biochemistry, University of California San Diego, La Jolla, California 92093, USA. E-mail: joelyuen@ucsd.edu

[b]Department of Chemistry, University of Chicago, 5735 S Ellis Ave, Chicago, Illinois 60637, USA

[c]Department of Chemistry, University of Wisconsin–Madison, Madison, Wisconsin 53706-1322, USA

† Electronic supplementary information (ESI) available. See DOI: https://doi.org/10.1039/d3sc01411h

strong illumination of a red-detuned laser can be a viable platform to achieve the long-standing goal of single and few-molecule vibrational polaritons. Few-molecule polaritons do not suffer from the deleterious effects of a macroscopic number of dark states, and hence are better candidates for harnessing the properties of polaritons.[5]

As a proof-of-concept application of few-molecule vibrational polaritons, we will introduce the intriguing concept of coupling chemical reactions *via* the latter. Biological systems use coupled chemical reactions and thermodynamics to their advantage by driving energetically uphill processes, such as active transport, using spontaneous reactions, like the dissociation of ATP.[58] Humans have looked towards nature for inspiration and translated biological knowledge into innovative products and processes.[59,60] We shall show how the delocalization of the polariton modes inside the cavity can be exploited to design a biomimetic of ATP-driven molecular machines.

Results and discussion

Model

Our theoretical model considers a single molecule in condensed phase placed inside a UV-vis cavity, such that the cavity frequency is off-resonant and lower than any optically allowed transitions of the molecule. In this regime, the coupling between the cavity and the molecule is purely parametric through the molecule's polarizability, with the vibration of the molecule causing a dispersive shift in the cavity resonance.[52] Due to better spatial overlap between the mode profile of the cavity and the molecule, we consider using a dielectric Fabry–Perót cavity. However, the formalism presented here is valid for other cavity types.[61,62] We show that the cavity-molecule system, when pumped with a laser, off-resonant to electronic transition of the molecule, and red-detuned from the cavity, with the detuning in the order of the molecule's vibrational frequency (Fig. 1b), yields an effective Hamiltonian resembling the vibrational polaritonic Hamiltonian. Importantly, the light-matter coupling can be tuned by varying the laser power. By deploying efficient off-resonant light-matter interactions, this scheme represents an attractive opportunity to explore strong light-matter coupling phenomena without worrying about resonant interactions that could induce deleterious photodamage of molecules.

In this setup, an anti-Stokes Raman process creates a composite photon mode by absorption of a red-detuned laser photon and subsequent emission of a cavity photon. When the laser-cavity detuning is parked at the vibrational frequency of the molecule, the composite photon is in resonance with the molecular vibration and couples to it (Fig. 1b), with an effective light-matter coupling strength that can be tuned by changing the laser intensity. When the coupling strength exceeds the decay rates of the system, we see polariton peaks in the spectra. Importantly, and contrary to the perturbative description of anti-Stokes Raman scattering, the presently studied effect occurs even at $T = 0$, in the absence of initial populations in the vibrational excited states of the molecules.

We model the photon mode and the vibration of the molecule as harmonic oscillators with frequencies ω_{cav} and Ω_v, and annihilation operators a and b, respectively. The cavity has a decay rate of κ and the vibrational mode has a decay rate of γ. In this work, the losses will be modeled using Lindblad master equations.[63] Since the polarizability, α, of the molecule, to the leading order, depends on its vibrational displacement,[56] $x_v = x_{zpf,v}(b^\dagger + b)$, the Hamiltonian for the cavity-molecule system is[52]

$$H_{C\text{-}M} = \hbar[\omega_{cav} + g_0(b^\dagger + b)]a^\dagger a + \hbar\Omega_v b^\dagger b, \quad (1)$$

where $g_0 = x_{zpf,v}\left(\omega_{cav}\frac{\partial\alpha}{\partial x_v}\frac{1}{\varepsilon_0 V_c}\right)$ is the vacuum cavity-molecule coupling, with V_c and ε_0 as the mode volume of the cavity and vacuum permittivity, respectively. This Hamiltonian formally resembles an optomechanical setup,[52] where the displacement of a mechanical oscillator modulates the frequency of the cavity. The cavity then acts back on the oscillator through radiation

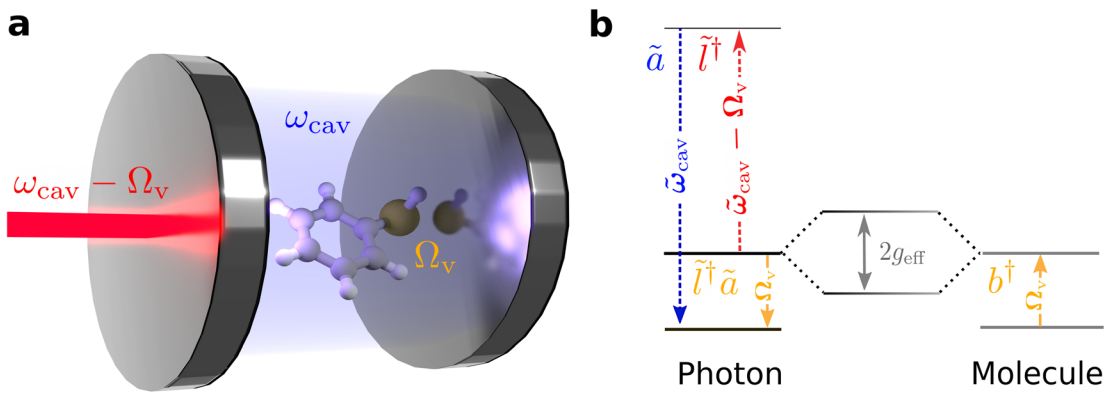

Fig. 1 Experimental setup for achieving few-molecule vibrational SC in a cavity-enhanced Raman spectroscopy (CERS) setup. (a) A single molecule with a vibrational mode at frequency Ω_v is placed inside a UV-vis cavity (ω_{cav}) and the cavity is illuminated with a laser red-detuned from the cavity ($\omega_{cav} - \Omega_v$). The cavity mode and the laser detuned to any electronic transition of the molecule. The laser and the cavity together constitute a composite photon mode that strongly couples to the vibrational mode of the molecule. (b) Schematic depicting the coupling of the composite photon mode denoted by annihilation operator $\tilde{l}^\dagger\tilde{a}$ with the molecular vibration denoted with annihilation operator b. Here $\tilde{l}$ denotes the 'laser-like' and $\tilde{a}$ denotes the 'cavity-like' normal mode of the laser-cavity subsystem. The composite photon mode and the molecular vibration strongly couple with effective coupling g_{eff}, to give the polaritons.

pressure force, which is a function of the cavity's photon occupation.

We drive the cavity with a laser red-detuned ($\omega_L = \omega_{cav} - \Delta$, $\Delta > 0$) from the cavity resonance. The full Hamiltonian for a laser mode with annihilation operator l coupled to the cavity-molecule subsystem is given as

$$H_{full} = H_{C\text{-}M} + \hbar\omega_L l^\dagger l + \hbar J(l^\dagger + l)(a^\dagger + a), \quad (2)$$

with the cavity-laser coupling $J = \sqrt{\frac{\kappa}{\tau_{rt_L}}}$. Here, τ_{rt_L} is related to the laser power $P = \frac{n_L \hbar\omega_L}{\tau_{rt_L}}$ with $n_L = \langle l^\dagger l\rangle$ being the mean photon number in the laser mode.[64]

We make the rotating wave approximation (RWA) in the laser-cavity coupling and diagonalize the laser-cavity subsystem. The operators $\tilde{l}$ and $\tilde{a}$ represent the new 'laser-like' and 'cavity-like' normal modes of the laser-cavity subsystem with frequencies $\tilde{\omega}_L$ and $\tilde{\omega}_{cav}$, respectively. The Hamiltonian after making the approximation and change of basis is

$$H_{full}^{RWA} = \hbar\Omega_v b^\dagger b + \hbar\tilde{\omega}_{cav}\tilde{a}^\dagger\tilde{a} + \hbar\tilde{\omega}_L\tilde{l}^\dagger\tilde{l} + \hbar g_0(\cos\varphi\cdot\tilde{a} + \sin\varphi\cdot\tilde{l})^\dagger(\cos\varphi\cdot\tilde{a} + \sin\varphi\cdot\tilde{l})(b^\dagger + b), \quad (3)$$

where $\varphi = \frac{1}{2}\tan^{-1}\left(\frac{2J}{\omega_{cav} - \omega_L}\right)$ is the laser-cavity mixing angle.[65]

Considering the red-detuned case for the cavity-laser detuning, Δ, in the order of $O(\Omega_v)$, we drop the off-resonant contributions in the cavity-molecule interaction term, simplifying H_{full} to

$$H_R = \hbar\Omega_v b^\dagger b + \hbar\tilde{\omega}_{cav}\tilde{a}^\dagger\tilde{a} + \hbar\tilde{\omega}_L\tilde{l}^\dagger\tilde{l} + \frac{\hbar g_0}{2}\sin(2\varphi)\cdot\tilde{l}^\dagger\tilde{a}b^\dagger + \tilde{l}^\dagger\tilde{a}^\dagger b. \quad (4)$$

We will later set the laser-cavity detuning $\Delta = \Omega_v$.

We define a composite laser-cavity photon mode with annihilation operator $\mathscr{A}_{ph} = \frac{\tilde{l}^\dagger\tilde{a}}{\sqrt{(\tilde{n}_L - \tilde{n}_a)}}$ (Fig. 1b), where $\tilde{n}_L = \langle\tilde{l}^\dagger\tilde{l}\rangle$ and $\tilde{n}_a = \langle\tilde{a}^\dagger\tilde{a}\rangle$ are the mean photon occupations in the 'laser-like' and 'cavity-like' normal modes, respectively. The Heisenberg equations of motion for the operators $\mathscr{A}_{ph}$ and b in the mean-field approximation,[66]

$$\frac{d}{dt}\mathscr{A}_{ph} = -i(\tilde{\omega}_{cav} - \tilde{\omega}_L)\mathscr{A}_{ph} - \frac{ig_0}{2}\sin(2\varphi)\sqrt{\tilde{n}_L - \tilde{n}_a}\cdot b, \quad (5a)$$

$$\frac{d}{dt}b = -i\Omega_v b - \frac{ig_0}{2}\sin(2\varphi)\sqrt{\tilde{n}_L - \tilde{n}_a}\cdot\mathscr{A}_{ph}, \quad (5b)$$

yield the effective Hamiltonian

$$H_{eff} \approx \hbar\omega_{ph}\mathscr{A}_{ph}^\dagger\mathscr{A}_{ph} + \hbar\Omega_v b^\dagger b + \hbar g_0\left(\frac{J}{\Delta}\right)\sqrt{n_L}\cdot\left(\mathscr{A}_{ph}^\dagger b + \mathscr{A}_{ph}b^\dagger\right), \quad (6)$$

when $n_L \gg \tilde{n}_a$ and $J \ll \Delta$ (see ESI note-1†). Here we have suggestively defined $\omega_{ph} \equiv \Delta$. For an input laser drive with power P, the interaction strength between the composite photon and the molecular vibration transforms to $g_{eff} = \frac{g_0}{\Delta}\sqrt{\frac{P\kappa}{\hbar\omega_L}}$, consistent with the results obtained from the classical treatments of the laser mode.[41,55,57,64]

When $\omega_{ph} = \Omega_v$, H_{eff} resembles a vibrational polaritonic Hamiltonian, where the composite photon mode is resonant with the vibrational DOF (Fig. 1b).[5] Here the coupling strength is tunable by changing the pumping power of the laser. This can, in principle, foster the SC regime when the coupling strength supersedes the decay processes in the system. To look at parameter sets yielding this regime and to compute spectra, we simulate the dynamics of the density matrix (ρ) of the system using Lindblad master equations[56,63] given as

$$\frac{\partial\rho}{\partial t} = i[H_{eff}, \rho] + \frac{\kappa}{2}\mathscr{L}_{\mathscr{A}}[\rho] + \frac{(n_v^{th} + 1)\gamma_r}{2}\mathscr{L}_b[\rho] + \frac{n_v^{th}\gamma_r}{2}\mathscr{L}_{b^\dagger}[\rho] + n_v^{th}\gamma_{pd}\mathscr{L}_{b^\dagger b}[\rho]. \quad (7)$$

The last four terms on the right-hand side are the Lindblad–Kossakowski terms defined as $\mathscr{L}_{\mathscr{O}}[\rho] = 2\mathscr{O}\rho\mathscr{O}^\dagger - \{\mathscr{O}^\dagger\mathscr{O}, \rho\}$. Here, $\mathscr{L}_{\mathscr{A}}$ models the incoherent decay from the composite photon mode. The incoherent decay, thermal pumping, and pure dephasing of the vibrational mode by the environment at temperature T are modeled by the $\mathscr{L}_b$, $\mathscr{L}_{b^\dagger}$ and $\mathscr{L}_{b^\dagger b}$ terms, respectively, where $n_v^{th} = (e^{\hbar\Omega_v/k_BT} - 1)^{-1}$ is the Bose–Einstein distribution function at transition energy $\hbar\Omega_v$. Additionally, in the limit of large photon number in the laser ($n_L \gg 1$), assuming the photon occupation to be constant, and thus the laser mode to be non-lossy, the decay rate of the composite photon equals the cavity decay rate κ (see ESI note-2†).

The simulations have been performed using the QuTip package[67,68] and the results are presented in Fig. 2 for the molecule Rhodamine 6G,[52] where $\hbar\Omega_v = 0.17$ eV, $\omega_{ph} = \Omega_v$ (0.17 eV), $\gamma = \gamma_r/2 + \gamma_{pd} = 0.01\Omega_v$ (1.7×10^{-3} eV), $\kappa = 0.02\Omega_v$ (3.4×10^{-3} eV), $g_0 = 1.5 \times 10^{-3}\Omega_v$ (2.6×10^{-4} eV). Here, $\gamma_r = 10^{-4}\Omega_v$ (1.7×10^{-5} eV) and γ_{pd} are the rates for vibrational relaxation and pure dephasing, respectively.[6] The temperature chosen for the simulations is $T = 298$ K. The fluence of the lasers is chosen to be below ~10 MW cm^{-2} (ref. 52 and 69) with a beam area of $A = 5$ μm^2. Fig. 2a shows the effective light-matter coupling, g_{eff}, as a function of laser fluence, P/A, and single photon coupling strength, g_0. In Fig. 2b, the vibrational spectrum of the molecule $S_b(\omega) = \mathrm{Re}[\int_0^\infty e^{-i\omega t}\langle x_v(t)x_v(0)\rangle_{ss}dt]$, splits, demonstrating SC. We see the Rabi-splitting increases with laser power, thus giving us additional control over the light-matter coupling strength. Fig. 2c shows the spectra with one, two, and four molecules for constant laser power. Fig. 2d is the vibrational spectrum of the molecule as a function of the cavity-laser detuning. The avoided crossing at the detuning (Δ) equal to the vibrational frequency (Ω_v) demonstrates maximal hybridization between the photonic and matter DOF. Finally, Fig. 2e and f show the emission spectra from the cavity at steady state (ss), $S_{\mathscr{A}}(\omega) = \omega^4\cdot\mathrm{Re}[\int_0^\infty e^{-i\omega t}\langle\mathscr{A}_{ph}^\dagger(t)\mathscr{A}_{ph}(0)\rangle_{ss}dt]$,[56,70,71] also revealing the polariton peaks.

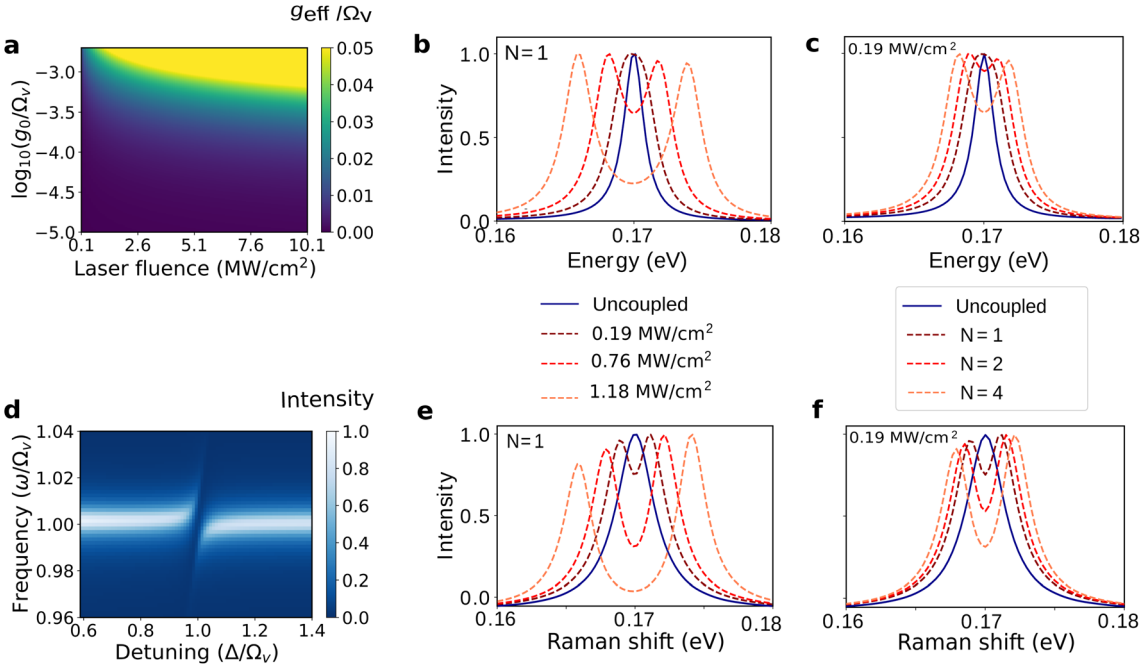

Fig. 2 Spectroscopic signatures of few-molecule vibrational strong coupling in CERS setup. (a) The effective light-matter coupling (g_{eff}) as a function of the single-photon coupling (g_0) and laser fluence. Vibrational spectra of the molecule as a function of (b) laser fluence, (c) the number of molecules (N), (d) cavity-laser detuning ($\omega_{\mathrm{cav}} - \omega_{\mathrm{L}} = \Delta$). Emission spectra from the cavity as a function of (e) laser fluence, (f) the number of molecules. Here $\hbar\Omega_{\mathrm{v}} = 0.17$ eV, $\omega_{\mathrm{cav}} = 1.7$ eV, $\omega_{\mathrm{ph}} = \Omega_{\mathrm{v}}$, $g_0 = 1.5 \times 10^{-3}\Omega_{\mathrm{v}}$, $\kappa = 0.02\Omega_{\mathrm{v}}$, $\gamma = \gamma_{\mathrm{r}}/2 + \gamma_{\mathrm{pd}} = 0.01\Omega_{\mathrm{v}}$, $\gamma_{\mathrm{r}}/2 = 10^{-4}\Omega_{\mathrm{v}}$, $T = 298$ K, and $A = 5$ μm^2 unless otherwise mentioned.

Polariton-assisted thermodynamic driving

The matter component of the polariton modes is delocalized over many molecules under collective SC.[5,72] This delocalization can be exploited more effectively with few-molecule polaritons, owing to reduced involvement of dark modes,[9,31] which remain parked essentially at the same energy as the original molecular transitions. In this work, we consider the molecular species undergoing electron-transfer reactions,[73,74] modeled using Marcus–Levich–Jortner (MLJ) theory.[75–77] Our system consists of two reactive molecules A and B of different species placed inside an optomechanical cavity. Here molecule A features a spontaneous reaction (with negative free energy change, $\Delta G_{\mathrm{A}} < 0$), while molecule B features an endergonic reaction ($\Delta G_{\mathrm{B}} > 0$, with $\Delta G_{\mathrm{B}} > k_{\mathrm{B}}T$). We demonstrate thermodynamic coupling between the two molecular species *via* the composite photon mode, such that the spontaneous electron transfer in A can drive B to react. Schematically, electron transfer in A creates a vibrationally hot product (Fig. 3a), which, outside the cavity, just decays to the product ground state. However, inside the cavity, in the timescale of the Rabi frequency, this excitation can be captured by the photon mode, which then can excite the reactant in B to its vibrational excited state. The electron transfer in B can then proceed spontaneously from the reactant's excited state (Fig. 3b). Notably, this scheme can also be generalized to other types of reactions. We emphasize that throughout this process there is no direct photoexcitation (preparation of vibrationally excited state population) of the molecules by light. This feature arises from the off-resonant nature of the parametrically induced strong light-matter coupling, and represents an opportunity to avoid undesired photochemical processes in molecules due to resonant multiphoton excitations.

Within the framework of MLJ theory, the molecules can exist in either of the two diabatic electronic states: $|R_i\rangle$ corresponding to the reactant and $|P_i\rangle$ corresponding to the product for molecule $i \in \{\mathrm{A}, \mathrm{B}\}$ (Fig. 3a). For molecule B, in this case the switching between $|R_{\mathrm{B}}\rangle$ and $|P_{\mathrm{B}}\rangle$ through electron transfer contributes to useful mechanical work, manifested in changes of nuclear configuration.[78–80] The electronic states for each molecule are dressed with a local high-frequency intramolecular vibrational coordinate represented by annihilation operator $a_{x,i}$, for $x \in \{R,P\}$, and coupled to a low-frequency effective solvent mode treated classically with rescaled momentum and position as $p_{\mathrm{S},i}$ and $q_{\mathrm{S},i}$. respectively. We assume that the high-frequency modes of both species, being resonant, are the only ones that couple to the composite photon.[81] Upon reaction, the high-frequency mode undergoes a change in its equilibrium configuration according to, $a_{\mathrm{R},i} = D_i^{\dagger} a_{\mathrm{P},i} D_i$, where $D_i = \exp[(a_{P,i}^{\dagger} - a_{P,i})\sqrt{S_i}]$ is the displacement operator, and S_i is the Huang–Rhys factor.[39] The Hamiltonian describing the system is given as $H = H_0 + V_{\mathrm{react}}$, where

$$H_0 = H_{\mathrm{ph}} + \sum_{i=A,B} \sum_{x=R,P} (H_{x,i} + V_{x,i})|x_i\rangle\langle x_i|, \tag{8a}$$

$$V_{\mathrm{react}} = \sum_{i=A,B} J_i(|R_i\rangle\langle P_i| + |P_i\rangle\langle R_i|). \tag{8b}$$

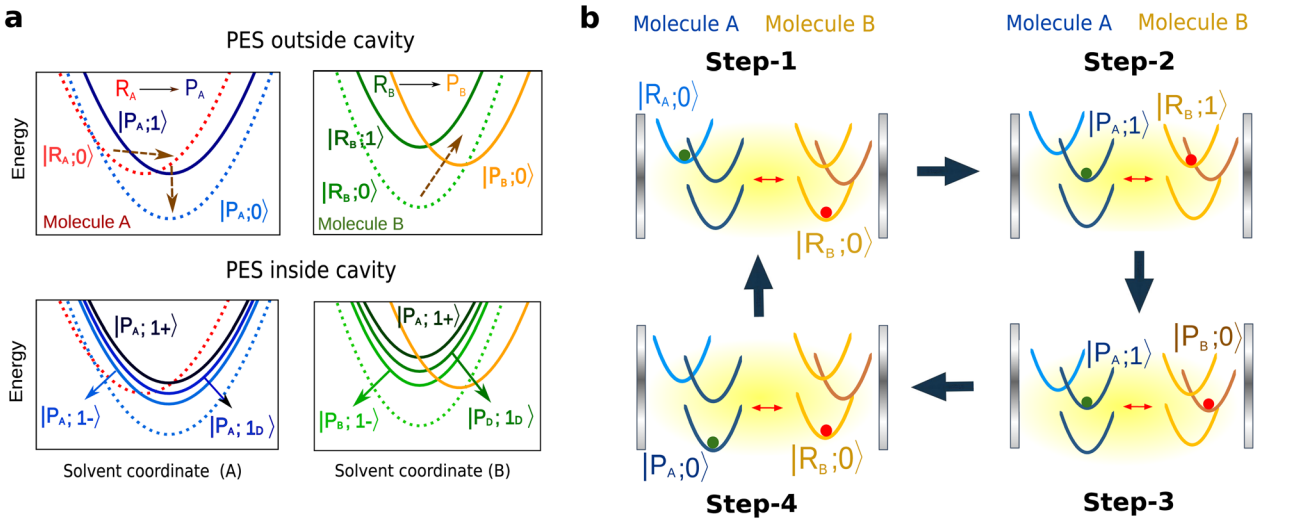

Fig. 3 (a) Schematic PES for molecules A and B, outside and inside the cavity. Both A and B undergo electron transfer reactions with negative and positive ΔG, respectively. The dashed arrows show the main reaction pathways for each molecule. The direction (upward or downward) of the arrow indicates whether the reaction is uphill or downhill and the steepness indicates the transition energy. The reaction takes molecule A from $|R_A\rangle$ to $|P_A\rangle$, and molecule B from $|R_B\rangle$ to $|P_B\rangle$. The PES are labeled as $|E,v_E\rangle$, where E labels the electronic state, R_i or P_i for $i \in \{A,B\}$. Outside the cavity, $|v_E\rangle$ represents the vibrational state of the high-frequency mode corresponding to the electronic state $|E\rangle$. The coupling of this high-frequency vibrational mode to the composite photon mode leads to the two polariton states, $|1_\pm\rangle$, and one dark state, $|1_D\rangle$. (b) One cycle of the coupled reactions. Step-1: we start from the reactant electronic states and vibrational ground states in both molecules ($|R_A;0\rangle$, $|R_B;0\rangle$). Step-2: as molecule A reacts spontaneously ($|R_A;0\rangle \rightarrow |P_A;1\rangle$), the polariton modes, $|P_A,R_B;1_\pm\rangle$, being delocalized also promote vibrational excitation in B from $|R_B;0\rangle$ to $|R_B;1\rangle$. Step-3: this allows B to react from its excited state ($|R_B;1\rangle \rightarrow |P_B;0\rangle$). Step-4: finally, both A and B relax to $|P_A;0\rangle$ and $|R_B;0\rangle$, respectively, after which the molecule A needs to be replaced for the next cycle (PES have been drawn not to scale, to emphasize the mechanism.).

Here $H_{\rm ph} = \hbar\omega_{\rm ph}\left(\mathscr{A}^\dagger_{\rm ph}\mathscr{A}_{\rm ph} + \frac{1}{2}\right)$ is the bare Hamiltonian corresponding to the composite photon mode consisting of the laser and the cavity, $H_{x,i}$ represents the high-frequency mode and the solvent mode associated with molecule x_i,

$$H_{R,i} = \hbar\Omega_{R,i}\left(a^\dagger_{R,i}a_{R,i} + \frac{1}{2}\right) + \frac{1}{2}\hbar\Omega_{S,i}\left(|p_{S,i}|^2 + |q_{S,i}|^2\right), \quad (9a)$$

$$H_{P,i} = \hbar\Omega_{P,i}\left(a^\dagger_{P,i}a_{P,i} + \frac{1}{2}\right) + \frac{1}{2}\hbar\Omega_{S,i}\left(|p_{S,i}|^2 + |q_{S,i} + d_{S,i}|^2\right) + \Delta G_i, \quad (9b)$$

with $d_{S,i}$ and $\Omega_{S,i}$ being the displacement and frequency along the solvent coordinate, respectively, and ΔG_i, the free energy difference for the molecular species i. Additionally, $V_{x,i} = \hbar g_{x,i}(a_{x,i}\mathscr{A}^\dagger_{\rm ph} + a^\dagger_{x,i}\mathscr{A}_{\rm ph})$ is the effective coupling between the photonic and molecular DOF. For simplicity, we assume that the reaction involves a vibrational mode with nearly identical frequency and light-matter coupling strength for species A and B in both the reactant and product electronic states ($\Omega_{x,i} = \Omega_{y,j} \equiv \Omega_v$ and $g_{x,i} = g_{y,j} \equiv g$). Finally, the diabatic couplings between the electronic states $|R_i\rangle$ and $|P_i\rangle$ are given by $V_{\rm react}$, where J_i is the coupling strength.

We can solve H_0 parametrically as a function of the solvent coordinates to construct the potential energy surfaces(PES) (Fig. 4a and b). Considering these diabatic couplings $V_{\rm react}$ to be perturbative, H_0 can be diagonalized to obtain the two polariton modes, $a^{(\pm)}_{x_A,y_B}$, with frequencies $\omega_\pm = \frac{1}{2}(\omega_{\rm ph} + \Omega_v \pm \sqrt{(\omega_{\rm ph} + \Omega_v)^2 + 8g^2})$, and one dark mode, $a^{D}_{x_A,y_B}$, with frequency Ω_v, given as

$$a^{(\pm)}_{x_A,y_B} = \cos\theta\,\mathscr{A}_{\rm ph} \pm \sin\theta\cdot\frac{1}{\sqrt{2}}\left(a_{x,A} + a_{y,B}\right), \quad (10a)$$

$$a^{D}_{x_A,y_B} = c_{x,A}a_{x,A} + c_{y,B}c_{y,B} \quad (10b)$$

such that, $c_{x,A} + c_{y,B} = 0$ and $|c_{x,A}|^2 + |c_{y,B}|^2 = 1$. Here, $\theta = \frac{1}{2}\tan^{-1}\left(\frac{2\sqrt{2}g}{\delta}\right)$ is the mixing angle, where $\delta = (\omega_{\rm ph} - \Omega_v)$ is the detuning between the composite photon mode and the molecule. Here we have chosen the composite photon mode to be resonant with the intramolecular vibration, *i.e.*, $\delta = 0$.

We now define multi-particle states $|\boldsymbol{\phi};\boldsymbol{\nu}_{\boldsymbol{\phi}}\rangle$ that span the Hilbert space of the system, where $|\boldsymbol{\phi}\rangle = |x_A, y_B\rangle$, $x, y \in \{R,P\}$ corresponds to the electronic DOF, and $|\boldsymbol{\nu}_{\boldsymbol{\phi}}\rangle = |\nu^+_{xA,yB},\nu^-_{xA,yB},\nu^D_{xA,yB}\rangle$ to the cavity-vibrational mode of each electronic state $|\boldsymbol{\phi}\rangle$.[6] To describe the reaction, we look at the population dynamics in the electronic states. The kinetic master equations governing the time evolution of the system are given as[6]

$$\frac{dp_{(\boldsymbol{\phi};\boldsymbol{\nu}_{\boldsymbol{\phi}})}(t)}{dt} = -\left[\sum_{\left(\boldsymbol{\phi}';\boldsymbol{\nu}'_{\boldsymbol{\phi}'}\right)\neq\left(\boldsymbol{\phi};\boldsymbol{\nu}_{\boldsymbol{\phi}}\right)} k\left(\boldsymbol{\phi}';\boldsymbol{\nu}'_{\boldsymbol{\phi}'}\middle|\boldsymbol{\phi};\boldsymbol{\nu}_{\boldsymbol{\phi}}\right)\right] p_{(\boldsymbol{\phi};\boldsymbol{\nu}_{\boldsymbol{\phi}})} + \sum_{\left(\boldsymbol{\phi}';\boldsymbol{\nu}'_{\boldsymbol{\phi}'}\right)\neq\left(\boldsymbol{\phi};\boldsymbol{\nu}_{\boldsymbol{\phi}}\right)} k\left(\boldsymbol{\phi};\boldsymbol{\nu}_{\boldsymbol{\phi}}\middle|\boldsymbol{\phi}';\boldsymbol{\nu}'_{\boldsymbol{\phi}'}\right)\cdot p_{\left(\boldsymbol{\phi}';\boldsymbol{\nu}'_{\boldsymbol{\phi}'}\right)}, \quad (11)$$

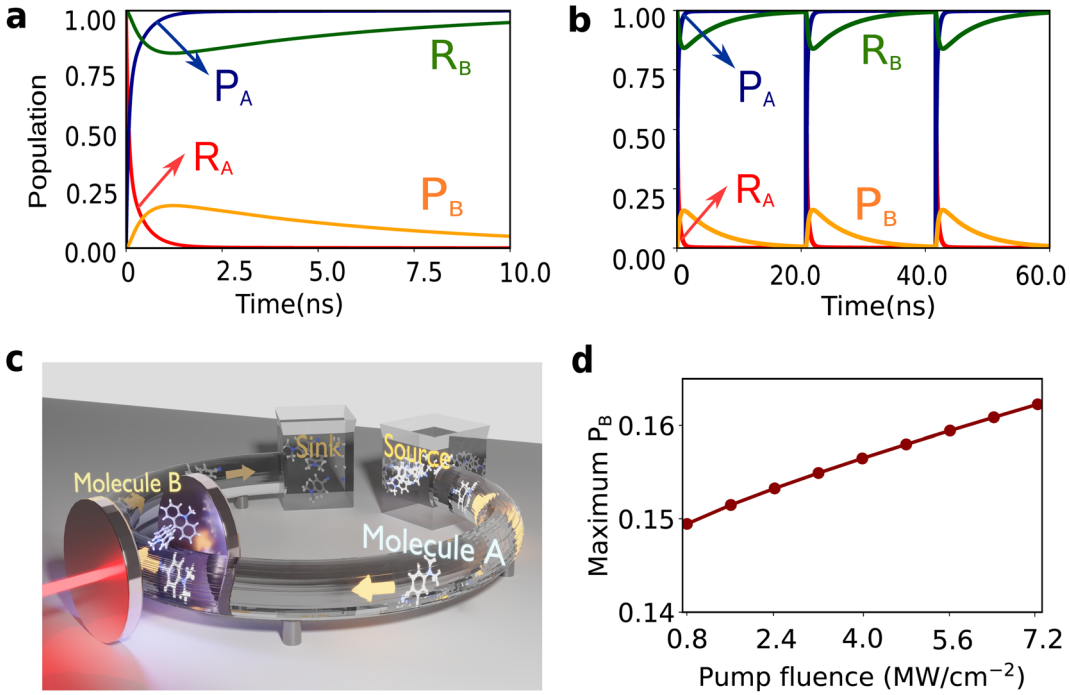

Fig. 4 Simulations showing polariton-assisted thermodynamic driving. Population dynamics of molecule A and B in (a) short times and (b) long times, with molecule A being replenished through the flow apparatus depicted in (c). Molecule B switches from $|R_B\rangle$ to $|P_B\rangle$ in a cycle, thus producing mechanical work. (c) Proposed experimental setup for continuous mechanical work from molecule B by the circulation of molecule A. Using a flow chemistry apparatus, molecule A in state $|R_A;0\rangle$ state (glowing) is transported from the 'source' bath to the cavity, where it transforms to $|P_A;0\rangle$ (no glow), drives molecule B from $|R_B;0\rangle$ to $|P_B;0\rangle$, and subsequently flow to the 'sink' bath. (d) Maximum population reached in P_B as a function of the fluence of the laser drive. Here $\hbar\Omega_{R,i} = \hbar\Omega_{P,i} = 0.22$ eV (call $\hbar\Omega_v$), $g_0 = 2\times10^{-3}\Omega_v$, $P/A = 1.1$ MW cm^{-2}, $A = 5$ μm^2, $\gamma_A = \gamma_B = 1\times10^{-5}\Omega_v$, $\omega_{cav} = 2.2$ eV, $\kappa = 0.015\Omega_v$, $\lambda_S^A = 0.04\hbar\Omega_v$, $\lambda_S^B = 0.1\hbar\Omega_v$, $\Delta G_A = -\hbar\Omega_v$, $\Delta G_B = 0.7\hbar\Omega_v$, $\hbar\Omega_{cut} = 0.1\hbar\Omega_v$, $T = 298$ K, and $\eta = 0.0001$ unless otherwise specified.

where $p_{(\phi;\nu_\phi)}(t)$ represents the population in $|\phi;\nu_\phi\rangle$ state, and $k(\phi';\nu'_{\phi'}|\phi;\nu_\phi)$ is the rate constant for population transfer from $|\phi;\nu_\phi\rangle$ to $|\phi';\nu''_\phi\rangle$ due to processes like reactive transitions between the electronic states accompanied by solvent reorganization and decay through the cavity and vibrational DOF. The rate constant for the reactive transition at a temperature T within the framework of MLJ theory is given as[81]

$$k\left(\phi';\nu'_{\phi'}|\phi;\nu_\phi\right) = \sqrt{\frac{\pi}{\lambda_S^{(\phi\phi')}k_BT}}\frac{|J_{(\phi\phi')}|^2}{\hbar}|\langle\nu'_{\phi'}|\nu_\phi\rangle|^2 \times\exp\left[-\frac{\left(E_{\phi;\nu\phi} - E_{\phi';\nu'_{\phi'}} + \lambda_S^{(\phi\phi')}\right)^2}{4\lambda_S^{(\phi\phi')}k_BT}\right] \quad (12)$$

Here,

$$E_{\phi;\nu_\phi} = E_{x_A} + E_{y_B} + \hbar\left[\omega_+\left(\nu^+_{x_Ay_B} + \frac{1}{2}\right) + \omega_-\left(\nu^-_{x_Ay_B} + \frac{1}{2}\right) + \Omega_v\left(\nu^D_{x_Ay_B} + \frac{1}{2}\right)\right]$$

is the energy of the state $|\phi;\nu_\phi\rangle = |x_A,y_B\rangle\otimes|\nu^+_{x_Ay_B},\nu^-_{x_Ay_B},\nu^D_{x_Ay_B}\rangle$, and $\lambda^{(\phi\phi')}$s and $J_{\phi\phi'}$ are the solvent reorganization energy and diabatic coupling, respectively, corresponding to the reacting species. Additionally, $\langle\nu'_{\phi'}|\nu_\phi\rangle$ represent the Franck–Condon factors for the hybrid photon-vibration states $|\nu'_{\phi'}\rangle$and $|\nu_\phi\rangle$ corresponding to the electronic states $|\phi'\rangle$ and $|\phi\rangle$, respectively. For the simulations in this work, the Franck–Condon factors have been computed numerically from eigenstates obtained using the standard discrete-variable representation (DVR) of Colbert and Miller.[82]

The reactive transitions transfer populations across different electronic states, while the cavity and vibrational decays lead to dynamics within the same electronic state. In these simulations, since $k_BT \ll \hbar\Omega_v$, we restrict ourselves to the first excitation manifold in the photon-vibration DOF. With the bare vibrational decay rate for the intramolecular vibrations for molecule A and B as γ_A and γ_B, respectively, and bare cavity decay rate as κ, we have

$$k(\phi,\mathbf{1}_{q,\phi}|\phi,\mathbf{0}) = |c_{q0}|^2\kappa + |c_{qA}|^2\gamma_A + |c_{qB}|^2\gamma_B, \quad (13)$$

where $\mathbf{1}_{q,\phi}$ represents a single excitation in the polaritons ($q = \pm$) or the dark ($q = D$) mode, and the c_{qj}'s correspond to the expansion coefficients of the excited eigenmode in terms of the cavity and vibrational modes.[83]

Finally, the anharmonic couplings between the vibrational mode of interest and an other bath of low frequency modes leads to transitions between the polaritons and the dark mode,[6]

$$k\left(\boldsymbol{\phi}, \mathbf{1}_{q,\boldsymbol{\phi}} \middle| \boldsymbol{\phi}, \mathbf{1}_{q',\boldsymbol{\phi}}\right) = 2\pi\left(\sum_{i=1}^{2} \left|c_{q'i}\right|^2 \left|c_{qi}\right|^2\right) \times \left\{\Theta(-\Omega)\cdot\left[n^{\mathrm{th}}(-\Omega)+1\right]\mathscr{J}(-\Omega) + \Theta(\Omega)n^{\mathrm{th}}(\Omega)\mathscr{J}(\Omega)\right\}, \quad (14)$$

where $\Theta(\Omega)$ is the heavyside step function, $n^{\mathrm{th}}(\Omega)$ is the Bose–Einstein distribution function at the transition energy $\hbar\Omega = \hbar(\Omega_{q'} - \Omega_q)$, and $\mathscr{J}(\Omega)$ is the spectral density of the low frequency modes. Assuming the spectral density to be ohmic,[84] we have $\mathscr{J}(\Omega) = \eta\Omega\exp[-(\Omega/\Omega_{\mathrm{cut}})^2]$, where η is a dimensionless parameter modeling the anharmonic system–bath interactions and Ω_{cut} is the cut-off frequency for the low-frequency modes.

The results of the simulations are presented in Fig. 4. Here, $\hbar\Omega_{\mathrm{R},i} = \hbar\Omega_{\mathrm{P},i} = 0.22$ eV (call $\hbar\Omega_{\mathrm{v}}$), $g_0 = 2\times10^{-3}\Omega_{\mathrm{v}}$ (4.4×10^{-4} eV), $P/A =$ 1.1 MW cm^{-2}, $A = 5$ μm^2, $\gamma_{\mathrm{A}} = \gamma_{\mathrm{B}} = 1\times10^{-5}\Omega_{\mathrm{v}}$ (2.2×10^{-6} eV),[6] $\omega_{\mathrm{cav}} = 2.2$ eV, $\kappa = 0.015\Omega_{\mathrm{v}}$ (3.3×10^{-3} eV), $\lambda_{\mathrm{S}}^{\mathrm{A}} = 0.04\hbar\Omega_{\mathrm{v}}$ (8.8×10^{-3} eV), $\lambda_{\mathrm{S}}^{\mathrm{B}} = 0.1\hbar\Omega_{\mathrm{v}}$ (2.2×10^{-2} eV), $\Delta G_{\mathrm{A}} = -\hbar\Omega_{\mathrm{v}}$ (−0.22 eV), $\Delta G_{\mathrm{B}} = 0.7\hbar\Omega_{\mathrm{v}}$ (0.15 eV), $\hbar\Omega_{\mathrm{cut}} = 0.1\hbar\Omega_{\mathrm{v}}$ (2.2×10^{-2} eV), and $\eta = 0.0001$.[6] The decay rates have been chosen to be similar to those typically found in VSC experiments.[66,85,86] The diabatic couplings are chosen to be $\hbar J_{\mathrm{A}} = \hbar J_{\mathrm{B}} = 0.005\hbar\Omega_{\mathrm{v}} =$($1.1\times10^{-3}$ eV) and $T = 298$ K. We start from the initial electronic state $|R_{\mathrm{A}},R_{\mathrm{B}};\mathbf{0}\rangle$. Independently, the reaction of molecule A is spontaneous due to its negative free energy change, $\Delta G_{\mathrm{A}} < 0$, while molecule B remains in its thermodynamically stable conformer $|R_{\mathrm{B}};0\rangle$ (Fig. 4a and b). This reflects the dynamics of the species outside of the cavity. Placing both the molecules inside the cavity couples the two reactions *via* the photonic mode enabling the spontaneity of the reaction of molecule A to thermodynamically 'lift' B to its unstable configuration $|P_{\mathrm{B}};0\rangle$ producing mechanical work. However, after molecule A has fully reacted (change in nuclear configuration), inevitably B has to relax again to its stable configuration $|R_{\mathrm{B}};0\rangle$, completing one cycle of the mechanical motion of B (Fig. 3b). The maximum population obtained in $|P_{\mathrm{B}}\rangle$ before molecule B relaxes back to $|R_{\mathrm{B}}\rangle$ increases with the light-matter coupling strength (g_{eff}), tunable with the fluence of the driving laser (Fig. 4d). For the cycle to be repeated, molecule A needs to be 'recharged' or 'replaced'. To achieve this, we envision a flow setup, as schematically depicted in Fig. 4c, that can circulate molecule A inside and out of the cavity. Continued circulation of the A molecules is essential for the molecular machine of B to be oscillating between reactant and product and producing mechanical work (Fig. 4a and b). This phenomenon realizes a heat engine producing mechanical work in molecule B, using the (chemical) energy flow from a 'source' to a 'sink' bath in the form of molecule A.[87]

Conclusion

We have shown that the physics of cavity optomechanics can be harnessed in CERS to achieve single to few-molecule vibrational SC using laser-driven UV-vis cavities. We show that the coupling strength and hence the Rabi splitting is tunable with the laser intensity, and it is achievable with realistic pump powers and cavity-molecule couplings. SC in the few molecules regime can avail enhanced polaritonic effects owing to the reduced entropic penalty from the dark states. By using the MLJ theory for electron transfer, we show that the photon-mediated coupling between two reactions, one spontaneous and one non-spontaneous, can be exploited to thermodynamically drive the non-spontaneous process using the spontaneous one. This effect is analogous to harnessing ATP to drive uphill biological processes like the active transport of ions across a membrane against their concentration gradient and can be used to design bio-inspired molecular machines.[88] Moving forward, an experimental realization of the scheme for vibrational SC presented here would be a significant step towards utilizing polaritons for chemistry.

Author contributions

A. K. designed, carried out, and analyzed the calculations. M. D. conceived the idea of polariton-assisted thermodynamic driving. S. P. S. and M. D. guided the design and analysis of the calculations. R. H. G. provided inputs on the experimental feasibility of the ideas conceived. J. Y. Z. designed, conceived, and supervised the project. A. K. wrote the paper with input from all other authors.

Conflicts of interest

The authors declare no competing interests.

Acknowledgements

This work was supported as part of the Center for Molecular Quantum Transduction (CMQT), an Energy Frontier Research Center funded by the U.S. Department of Energy, Office of Science, Basic Energy Sciences under Award No. DE-SC0021314. A.K. thanks Yong Rui Poh, Kai Schwenickke, Juan B. Pérez-Sánchez, Alex Fairhall, and Carlos A. Saavedra Salazar for useful discussions.

Notes and references

1 A. Kavokin, J. Baumberg, G. Malpuech and F. Laussy, *Microcavities*, OUP Oxford, 2017.
2 P. Törmä and W. L. Barnes, *Rep. Prog. Phys.*, 2014, **78**, 013901.
3 O. Bitton, S. N. Gupta and G. Haran, *Nanophotonics*, 2019, **8**, 559–575.
4 M. R. Bourgeois, E. K. Beutler, S. Khorasani, N. Panek and D. J. Masiello, *Phys. Rev. Lett.*, 2022, **128**, 197401.
5 R. F. Ribeiro, L. A. Martínez-Martínez, M. Du, J. Campos-Gonzalez-Angulo and J. Yuen-Zhou, *Chem. Sci.*, 2018, **9**, 6325–6339.
6 M. Du, J. A. Campos-Gonzalez-Angulo and J. Yuen-Zhou, *J. Chem. Phys.*, 2021, **154**, 084108.
7 A. D. Dunkelberger, B. S. Simpkins, I. Vurgaftman and J. C. Owrutsky, *Annu. Rev. Phys. Chem.*, 2022, **73**, 429–451.
8 K. Hirai, J. A. Hutchison and H. Uji-i, *ChemPlusChem*, 2020, **85**, 1981–1988.
9 M. Du and J. Yuen-Zhou, *Phys. Rev. Lett.*, 2022, **128**, 096001.
10 M. D. Fraser, *Semicond. Sci. Technol.*, 2017, **32**, 093003.
11 P. Berini and I. De Leon, *Nat. Photonics*, 2012, **6**, 16–24.
12 O. Jamadi, F. Reveret, P. Disseix, F. Medard, J. Leymarie, A. Moreau, D. Solnyshkov, C. Deparis, M. Leroux,

E. Cambril, S. Bouchoule, J. Zuniga-Perez and G. Malpuech, *Light: Sci. Appl.*, 2018, **7**, 82.
13 H. S. Nguyen, D. Vishnevsky, C. Sturm, D. Tanese, D. Solnyshkov, E. Galopin, A. Lemaître, I. Sagnes, A. Amo, G. Malpuech and J. Bloch, *Phys. Rev. Lett.*, 2013, **110**, 236601.
14 F. Marsault, H. S. Nguyen, D. Tanese, A. Lemaître, E. Galopin, I. Sagnes, A. Amo and J. Bloch, *Appl. Phys. Lett.*, 2015, **107**, 201115.
15 A. Amo, T. C. H. Liew, C. Adrados, R. Houdré, E. Giacobino, A. V. Kavokin and A. Bramati, *Nat. Photonics*, 2010, **4**, 361–366.
16 F. Chen, H. Li, H. Zhou, S. Luo, Z. Sun, Z. Ye, F. Sun, J. Wang, Y. Zheng, X. Chen, H. Xu, H. Xu, T. Byrnes, Z. Chen and J. Wu, *Phys. Rev. Lett.*, 2022, **129**, 057402.
17 M. Wang, M. Hertzog and K. Börjesson, *Nat. Commun.*, 2021, **12**, 1874.
18 M. Du, L. A. Martínez-Martínez, R. F. Ribeiro, Z. Hu, V. M. Menon and J. Yuen-Zhou, *Chem. Sci.*, 2018, **9**, 6659–6669.
19 G. Groenhof and J. J. Toppari, *J. Phys. Chem. Lett.*, 2018, **9**, 4848–4851.
20 A. Thomas, L. Lethuillier-Karl, K. Nagarajan, R. M. A. Vergauwe, J. George, T. Chervy, A. Shalabney, E. Devaux, C. Genet, J. Moran and T. W. Ebbesen, *Science*, 2019, **363**, 615–619.
21 K. Hirai, R. Takeda, J. A. Hutchison and H. Uji-i, *Angew. Chem., Int. Ed.*, 2020, **59**, 5332–5335.
22 M. Du, R. F. Ribero and J. Yuen-Zhou, *Chem*, 2019, **5**, 1167–1181.
23 T. S. Haugland, E. Ronca, E. F. Kjønstad, A. Rubio and H. Koch, *Phys. Rev. X*, 2020, **10**, 041043.
24 D. Sidler, C. Schäfer, M. Ruggenthaler and A. Rubio, *J. Phys. Chem. Lett.*, 2021, **12**, 508–516.
25 D. N. Basov, A. Asenjo-Garcia, P. J. Schuck, X. Zhu and A. Rubio, *Nanophotonics*, 2021, **10**, 549–577.
26 M. A. May, D. Fialkow, T. Wu, K.-D. Park, H. Leng, J. A. Kropp, T. Gougousi, P. Lalanne, M. Pelton and M. B. Raschke, *Adv. Quantum Technol.*, 2020, **3**, 1900087.
27 T. E. Li, B. Cui, J. E. Subotnik and A. Nitzan, *Annu. Rev. Phys. Chem.*, 2022, **73**, 43–71.
28 J. A. Campos-Gonzalez-Angulo, Y. R. Poh, M. Du and J. Yuen-Zhou, *J. Chem. Phys.*, **21**, 230901.
29 J. Keeling and S. Kéna-Cohen, *Annu. Rev. Phys. Chem.*, 2020, **71**, 435–459.
30 E. Cortese, P. G. Lagoudakis and S. De Liberato, *Phys. Rev. Lett.*, 2017, **119**, 043604.
31 R. Chikkaraddy, B. de Nijs, F. Benz, S. J. Barrow, O. A. Scherman, E. Rosta, A. Demetriadou, P. Fox, O. Hess and J. J. Baumberg, *Nature*, 2016, **535**, 127–130.
32 A. V. Zasedatelev, A. V. Baranikov, D. Urbonas, F. Scafirimuto, U. Scherf, T. Stöferle, R. F. Mahrt and P. G. Lagoudakis, *Nat. Photonics*, 2019, **13**, 378–383.
33 S. Kéna-Cohen and S. R. Forrest, *Nat. Photonics*, 2010, **4**, 371–375.
34 J. J. Baumberg, A. V. Kavokin, S. Christopoulos, A. J. D. Grundy, R. Butté, G. Christmann, D. D. Solnyshkov, G. Malpuech, G. Baldassarri Höger von Högersthal, E. Feltin, J.-F. Carlin and N. Grandjean, *Phys. Rev. Lett.*, 2008, **101**, 136409.
35 S. Ghosh and T. C. H. Liew, *Npj Quantum Inf.*, 2020, **6**, 16.
36 M. Pelton, S. D. Storm and H. Leng, *Nanoscale*, 2019, **11**, 14540–14552.
37 A. Pscherer, M. Meierhofer, D. Wang, H. Kelkar, D. Martín-Cano, T. Utikal, S. Götzinger and V. Sandoghdar, *Phys. Rev. Lett.*, 2021, **127**, 133603.
38 D. Wang, H. Kelkar, D. Martin-Cano, T. Utikal, S. Götzinger and V. Sandoghdar, *Phys. Rev. X*, 2017, **7**, 021014.
39 S. Pannir-Sivajothi, J. A. Campos-Gonzalez-Angulo, L. A. Martínez-Martínez, S. Sinha and J. Yuen-Zhou, *Nat. Commun.*, 2022, **13**, 1645.
40 M. Mondal, A. Semenov, M. A. Ochoa and A. Nitzan, *J. Phys. Chem. Lett.*, 2022, **13**, 9673–9678.
41 M. Aspelmeyer, T. J. Kippenberg and F. Marquardt, *Rev. Mod. Phys.*, 2014, **86**, 1391–1452.
42 F. Elste, S. M. Girvin and A. A. Clerk, *Phys. Rev. Lett.*, 2009, **102**, 207209.
43 C. H. Metzger and K. Karrai, *Nature*, 2004, **432**, 1002–1005.
44 F. Massel, T. T. Heikkilä, J.-M. Pirkkalainen, S. U. Cho, H. Saloniemi, P. J. Hakonen and M. A. Sillanpää, *Nature*, 2011, **480**, 351–354.
45 A. A. Clerk, M. H. Devoret, S. M. Girvin, F. Marquardt and R. J. Schoelkopf, *Rev. Mod. Phys.*, 2010, **82**, 1155–1208.
46 B. Patra, B. Kafle and T. G. Habteyes, *Nano Lett.*, 2023, **23**(11), 5108–5115.
47 M. Fleischhauer, A. Imamoglu and J. P. Marangos, *Rev. Mod. Phys.*, 2005, **77**, 633–673.
48 A. H. Safavi-Naeini, T. P. M. Alegre, J. Chan, M. Eichenfield, M. Winger, Q. Lin, J. T. Hill, D. E. Chang and O. Painter, *Nature*, 2011, **472**, 69–73.
49 M. Rashid, T. Tufarelli, J. Bateman, J. Vovrosh, D. Hempston, M. S. Kim and H. Ulbricht, *Phys. Rev. Lett.*, 2016, **117**, 273601.
50 H. Tan, G. Li and P. Meystre, *Phys. Rev. A*, 2013, **87**, 033829.
51 S. Gröblacher, K. Hammerer, M. R. Vanner and M. Aspelmeyer, *Nature*, 2009, **460**, 724–727.
52 P. Roelli, C. Galland, N. Piro and T. J. Kippenberg, *Nat. Nanotechnol.*, 2016, **11**, 164–169.
53 M. K. Schmidt, R. Esteban, F. Benz, J. J. Baumberg and J. Aizpurua, *Faraday Discuss.*, 2017, **205**, 31–65.
54 Y. Zhang, J. Aizpurua and R. Esteban, *ACS Photonics*, 2020, **7**, 1676–1688.
55 T. Neuman, R. Esteban, G. Giedke, M. K. Schmidt and J. Aizpurua, *Phys. Rev. A*, 2019, **100**, 043422.
56 M. K. Schmidt, R. Esteban, A. González-Tudela, G. Giedke and J. Aizpurua, *ACS Nano*, 2016, **10**, 6291–6298.
57 R. Esteban, J. J. Baumberg and J. Aizpurua, *Acc. Chem. Res.*, 2022, **55**, 1889–1899.
58 I. Tinoco, K. Sauer, J. Wang, J. Puglisi, G. Harbison and D. Rovnyak, *Physical Chemistry: Principles and Applications in Biological Sciences*, Pearson Education, 2013.
59 R. Breslow, *J. Biol. Chem.*, 2009, **284**, 1337–1342.
60 Y. Hong, D. Velegol, N. Chaturvedi and A. Sen, *Phys. Chem. Chem. Phys.*, 2010, **12**, 1423–1435.
61 I. Shlesinger, K. G. Cognée, E. Verhagen and F. A. Koenderink, *ACS Photonics*, 2021, **8**(12), 3506–3516.

62 M. Tokman, M. Erukhimova, Q. Chen and A. Belyanin, *Phys. Rev. A*, 2022, **105**(5), 053707.
63 A. Nitzan, *Chemical Dynamics in Condensed Phases: Relaxation, Transfer, and Reactions in Condensed Molecular Systems*, OUP Oxford, 2013, ch. 10.
64 D. Steck, *Quantum and Atom Optics*, 2007, ch. 12, pp. 509–518.
65 A. Mandal, T. D. Krauss and P. Huo, *J. Phys. Chem. B*, 2020, **124**, 6321–6340.
66 R. F. Ribeiro, A. D. Dunkelberger, B. Xiang, W. Xiong, B. S. Simpkins, J. C. Owrutsky and J. Yuen-Zhou, *J. Phys. Chem. Lett.*, 2018, **9**, 3766–3771.
67 J. Johansson, P. Nation and F. Nori, *Comput. Phys. Commun.*, 2012, **183**, 1760–1772.
68 J. Johansson, P. Nation and F. Nori, *Comput. Phys. Commun.*, 2012, **183**, 1760–1772.
69 D. Werner and S. Hashimoto, *J. Phys. Chem. C*, 2011, **115**, 5063–5072.
70 P. Johansson, H. Xu and M. Käll, *Phys. Rev. B*, 2005, **72**, 035427.
71 M. K. Dezfouli, R. Gordon and S. Hughes, *ACS Photonics*, 2019, **6**, 1400–1408.
72 A. D. Dunkelberger, B. S. Simpkins, I. Vurgaftman and J. C. Owrutsky, *Annu. Rev. Phys. Chem.*, 2022, **73**, 429–451.
73 S. Hammes-Schiffer, *J. Am. Chem. Soc.*, 2015, **137**, 8860–8871.
74 G. A. Parada, Z. K. Goldsmith, S. Kolmar, B. P. Rimgard, B. Q. Mercado, L. Hammarström, S. Hammes-Schiffer and J. M. Mayer, *Science*, 2019, **364**, 471–475.
75 R. A. Marcus, *Annu. Rev. Phys. Chem.*, 1964, **15**, 155–196.
76 V. Levich, *Adv. Electrochem. Electrochem. Eng.*, 1966, **4**, 249–371.
77 J. Jortner, *J. Chem. Phys.*, 1976, **64**, 4860–4867.
78 J. M. Abendroth, O. S. Bushuyev, P. S. Weiss and C. J. Barrett, *ACS Nano*, 2015, **9**, 7746–7768.
79 E. Ahlberg, O. Hammerich and V. D. Parker, *J. Am. Chem. Soc.*, 1981, **103**, 844–849.
80 B. A. Olsen and D. H. Evans, *J. Am. Chem. Soc.*, 1981, **103**, 839–843.
81 J. A. Campos-Gonzalez-Angulo, R. F. Ribeiro and J. Yuen-Zhou, *Nat. Commun.*, 2019, **10**, 4685.
82 D. T. Colbert and W. H. Miller, *J. Chem. Phys.*, 1992, **96**, 1982–1991.
83 J. J. Hopfield, *Phys. Rev.*, 1969, **182**, 945–952.
84 J. del Pino, J. Feist and F. J. Garcia-Vidal, *New J. Phys.*, 2015, **17**, 053040.
85 B. Xiang, R. F. Ribeiro, A. D. Dunkelberger, J. Wang, Y. Li, B. S. Simpkins, J. C. Owrutsky, J. Yuen-Zhou and W. Xiong, *Proc. Natl. Acad. Sci. U. S. A.*, 2018, **115**, 4845–4850.
86 B. Xiang, R. F. Ribeiro, M. Du, L. Chen, Z. Yang, J. Wang, J. Yuen-Zhou and W. Xiong, *Science*, 2020, **368**, 665–667.
87 C. Morris, *The Dawn of Innovation*: The First American Industrial Revolution, 2012, p. 42.
88 V. Richards, *Nat. Chem.*, 2016, **8**, 1090.